Seventh International Conference on Computational Fluid Dynamics (ICCFD7), Big Island, Hawaii, July 9-13, 2012

ICCFD7-2012-2205

Flux Functions for Reducing Numerical Shockwave Anomalies

Daniel W. Zaide and Philip L. Roe
Corresponding Author: zaidedan@umich.edu

Department of Aerospace Engineering, University of Michigan,
Ann Arbor, Michigan, USA, 48109.

Abstract: Numerical shockwave anomalies for the Euler equations are directly related to the nonlinearity of the jump conditions and ambiguity of sub-cell shock position. In this work, two new flux functions are described that allow stationary shocks with no positional ambiguity. These functions are tested on several common model problems. In one dimension, they are shown to virtually eliminate both the carbuncle and slowly moving shockwave phenomena and reduce wall heating by as much as 60% with no loss of shock resolution and minimal effects to smooth regions of the flow.

Keywords: Numerical Algorithms, Computational Fluid Dynamics, Shock-Capturing, Flux Functions, Numerical Shockwave Anomalies.

1 Introduction

When a physical shockwave is formed, it moves through the flow with a certain speed, having some finite width determined by physical dissipation until it encounters some event in its path. For numerical shockwaves, however, a numerical width is enforced, often much greater than the physical width. With this numerical width comes the formation of intermediate states having no direct physical interpretation. Even as the mesh is refined, these intermediate states do not go away; they simply occupy less space. The existence of these intermediate states does raise some doubt, however, about how closely a captured shockwave may emulate an ideal discontinuous shockwave, or a real physical one.

There are in fact several types of error associated with intermediate shock states such as errors in shock position, spurious waves, or unstable shock behavior. These errors can be classified as *numerical shockwave anomalies*, numerical artifacts formed due to the presence of captured shockwaves within the flow solution. One of the first accounts of anomalous behavior was by in 1966 by Cameron [1], using a similar method to that of von Neumann and Richtmyer, who observed oscillations produced when shockwaves crossed both grid and material interfaces. He suggested that either the artificial viscosity or the mesh should be modified to properly smear out the shock. Two years later Emery [2] identified errors produced by shockwaves and again, suggested adding additional viscosity. As new shock capturing schemes were being developed, anomalous behavior was more frequently observed and was classified into several main categories.

Slowly Moving Shockwaves

The slowly moving shockwave phenomenon is the shedding of spurious waves by slowly moving shocks. The first detailed study of slowly moving shocks was by Roberts, [3] who examined the intermediate shock states and noted their role in the creation of spurious waves. Similar work by Arora and Roe [4] would follow up on this idea, studying a range of problems and the role of intermediate states, relating the problem to an error in the stationary shock structure. The consensus in the literature [5, 6, 7, 8, 9, 10, 11, 12] is that the root cause of these post shock oscillations is the unsteadiness of the discrete profile and the inability of any existing scheme to add what is deemed to be the 'correct' artificial viscosity. Xu [13] even went as far as to suggest that getting the viscosity correct was impossible, and no scheme of the type would ever work. Other researchers have not been as negative, developing various forms of artificial viscosity and showing fairly positive results. However, nobody to date has succeeded in eliminating the errors without smearing the shock .

The Carbuncle

Another anomaly, first described by Peery and Imlay [14] as an irregular shock behavior around a blunt body, the carbuncle has since been replicated in other situations [15]. Specifically, Quirk [16] introduced the most commonly analysed version, consisting of a one-dimensional shock in a two-dimensional domain. By perturbing the shock, in his case through the grid, an instability is provoked and a shock behavior similar to that of the original carbuncle is observed. An even simpler version of the problem has also been analysed [17, 18], in the form of a one-dimensional stationary shock that can develop spontaneous instabilities on a two-dimensional grid. Looking back to classical theory, Dyakov [19] and Landau and Livschitz [20] showed that the exact stationary shockwave was always stable, at least for convex equations of state. This demonstrates that captured shocks do not in fact share all of the properties of an ideal shock, even under mesh refinement, because no reference length is involved.

For numerical shockwaves, the analysis has most often taken the form of a linearized stability analysis, examining the stability of perturbations to the flow field [21, 22, 23, 24, 25, 26]. This has resulted in a wide range of theories about possible causes, from too much numerical vorticity [27, 28] to the conjecture of Liou [29], that flux functions where the mass flux is not a function of the pressure jump will not suffer from the carbuncle or other instabilities. Flux functions of this type are not physical, and were later shown to suffer from carbuncles [27, 18]. The carbuncle has been especially linked with schemes that exactly capture contact discontinuities and shear waves [23, 24]. This is unfortunate, since such schemes are important for the extension to viscous flows.

A difficulty with eliminating carbuncles is that they are physical solutions, 'mimicking' experimentally observable behavior [30, 31]. More recently, Elling [32] went so far as to suggest that since carbuncles are entropy-satisfying solutions, to eliminate them would be making unjustifiable physical assumptions and they are thus incurable. Although this a valid point, it seems that Nature usually selects against carbuncles, and it is reasonable to hope for a numerical scheme that selects in the same way.

The Wall Heating Phenomenon

A third anomaly is the creation of persistent "entropy traces" caused by an inappropriate production of entropy which then propagates in a physical manner [33, 34]. One such example, the wall heating phenomenon exemplified by Noh's [35, 9] well known test problem has caused much grief, both in the Eulerian and Lagrangian communities and occurs for a wide range of methods and physics [36]. This problem is again exacerbated by methods that capture contact discontinuities [37]. These also capture errors along contacts and are generally less diffusive.

Similar to Noh's original remedy, artificial heat conduction has been used in several other methods to alleviate the temperature excess[37, 38, 39], although much like Noh's original work, these tend to smear out other flow features. There have also been shock fitting attempts [40, 41] which have shown good results on the Noh problem. These, however, still suffer from the standard challenges of shock fitting approaches.

Relationship among anomalies

It has been previously postulated by Barth [21] and Robinet et al. [23] among others [42, 43, 10] that many of these numerical problems are related. We previously demonstrated that these problems were linked through the nonlinearity of the jump conditions and the resulting ambiguity in sub-cell shock position [44]. We have focussed in our work in eliminating the positional ambiguity in the special case of a stationary shock, and we find a class of schemes that achieves this without sacrificing shock resolution. The other anomalies turn out to be reduced, although by varying amounts.

2 Finite-Volume Method

We study systems of hyperbolic conservation equations in one dimension of the form

$$\mathbf{u}_t + \mathbf{f}_x = \mathbf{0} \tag{1}$$

with conserved variables $\mathbf{u}$ and fluxes $\mathbf{f}$. We assume that this system is complete with diagonalizable flux Jacobian $\mathbf{A} = \frac{\partial \mathbf{f}}{\partial \mathbf{u}}$ allows for weak solutions satisfying the jump conditions, $\Delta\mathbf{f} = S\Delta\mathbf{u}$ for a discontinuity with speed S. We discretize over a finite volume cell in space and time using the first-order upwind spatial discretization and the first-order explicit timestepping scheme on cell-averaged piecewise constant data to get the standard method

$$\mathbf{u}_i^{n+1} = \mathbf{u}_i^n - \frac{\Delta t}{\Delta x}\left(\mathbf{f}^n_{i+\frac{1}{2}} - \mathbf{f}^n_{i-\frac{1}{2}}\right) \tag{2}$$

where the interface flux, $\mathbf{f}_{i+\frac{1}{2}} = \mathbf{f}(\mathbf{u}_i, \mathbf{u}_{i+1})$, is computed using a Riemann solver. We restrict ourselves to first-order for now as not only does it simplicity lead to a range of analysis but experience suggests that increased accuracy does not alleviate the problems found in the first-order method.

2.1 Roe's Approximate Riemann Solver

We will make use of Roe's approximate Riemann solver throughout this work. This is in part because its simplicity is conducive to analysis, partly because in the majority of cases it gives results almost indistinguishable from the exact Riemann solution, and partly because it introduces itself anyway, as a necessary ingredient of our cure. Let us define it here for clarity. Given a left state $\mathbf{u}_i$ and a right state $\mathbf{u}_{i+1}$, the flux between them is

$$\mathbf{f}_{i+\frac{1}{2}} = \frac{1}{2}(\mathbf{f}_i + \mathbf{f}_{i+1}) - \frac{1}{2}|\tilde{\mathbf{A}}_{i+\frac{1}{2}}(\mathbf{u}_i, \mathbf{u}_{i+1})|(\mathbf{u}_{i+1} - \mathbf{u}_i) \tag{3}$$

and the approximate flux Jacobian $\tilde{\mathbf{A}}(\mathbf{u}_i, \mathbf{u}_{i+1})$ is constructed with the following properties: eigenvalue decomposition $\tilde{\mathbf{A}} = \tilde{\mathbf{R}}\tilde{\mathbf{\Lambda}}\tilde{\mathbf{L}}$ with real eigenvalues and linearly independent eigenvectors, consistency $\tilde{\mathbf{A}}(\mathbf{u}, \mathbf{u}) = \mathbf{A}(\mathbf{u})$, and conservation across discontinuities, $\mathbf{f}_{i+1} - \mathbf{f}_i = \tilde{\mathbf{A}}(\mathbf{u}_{i+1} - \mathbf{u}_i)$. This final

property leads to the flux wave description of Roe's approximate Riemann solver,

$$\mathbf{f}_{i+\frac{1}{2}} = \frac{1}{2}(\mathbf{f}_i + \mathbf{f}_{i+1}) - \frac{1}{2}\text{sign}(\tilde{\mathbf{A}}_{i+\frac{1}{2}}(\mathbf{u}_i, \mathbf{u}_{i+1}))(\mathbf{f}_{i+1} - \mathbf{f}_i) \tag{4}$$

which is used in subsequent sections.

3 Euler Equations

The main physical model we are interested in in this work are the Euler equations for inviscid, compressible flow. They will serve as the basis for the numerical experiments performed in this work, but the theory could be applied to arbitrary systems. The Euler equations represent the conservation of mass, momentum, and energy

$$\frac{\partial}{\partial t}\begin{bmatrix} \rho \\ \rho u \\ E \end{bmatrix} + \frac{\partial}{\partial x}\begin{bmatrix} \rho u \\ \rho u^2 + p \\ \rho u H \end{bmatrix} = \mathbf{0} \tag{5}$$

where enthalpy $H = \frac{E+p}{\rho}$. It is crucial to our understanding of the shock anomalies that this system is not closed until the pressure has been defined through an equation of state. For an ideal gas in thermodynamic equilibrium, the equation of state is

$$p = (\gamma - 1)\rho e = (\gamma - 1)\left(E - \frac{1}{2}\rho u^2\right). \tag{6}$$

where γ is the polytropic constant, the ratio of specific heats.

To describe shockwaves, the jump conditions are used. For waves corresponding to $\lambda = u + a$, suppose that the left (preshock) state is completely known, as ρ_L, u_L, p_L. If the density on the right is prescribed to be ρ_R, then the remaining postshock variables are given in [45] by

$$p_R = p_L \frac{(\gamma+1)\rho_R - (\gamma-1)\rho_L}{(\gamma+1)\rho_L - (\gamma-1)\rho_R} \tag{7}$$

$$u_R = u_L + (p_L - p_R)\sqrt{\frac{2}{\rho_L\left((\gamma-1)p_L + (\gamma+1)p_R\right)}} \tag{8}$$

with the shock speed as

$$S = u_L + a_L\sqrt{1 + \frac{\gamma+1}{2\gamma}\left(\frac{p_R}{p_L} - 1\right)}. \tag{9}$$

The curve traced out in phase space by solving these equations is the Hugoniot curve. It has two branches. If $\rho_R > \rho_L$ then each point on the curve represents a valid state behind a (generally moving) shockwave, and this will be referred to as the *physical branch* of the Hugoniot curve. If $\rho_R < \rho_L$ this generates the *nonphysical branch* of the Hugoniot. A jump from $\mathbf{u}_L$ to $\mathbf{u}_R$ would violate thermodynamics. Note however, that each point on the nonphysical branch represents a state from which $\mathbf{u}_L$ could be reached by a valid shockwave. Typical Hugoniot curves are shown in Figure 1, demonstrating the differences between the two branches of the Hugoniot.

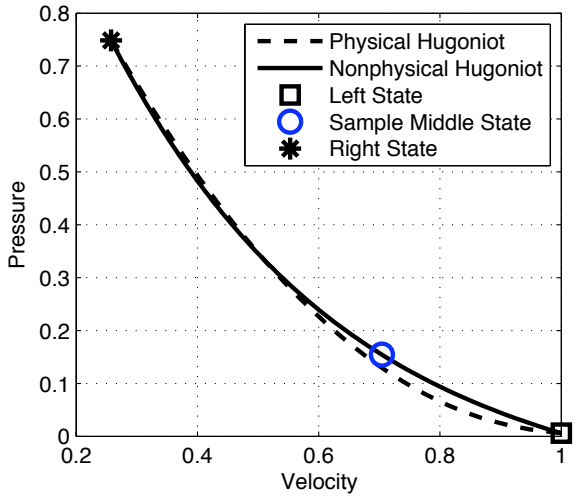

Figure 1: Typical Hugoniot curves for the stationary shock in the Euler equations. The physical Hugoniot is plotted through through L and the nonphysical Hugoniot through R. (Note that the curves are really in three-dimensional space, and do not actually intersect.)

4 An Ambiguity in Shock Position

Shock capturing arises from the observation that if no special measures are taken to incorporate shocks into a calculation, they tend to appear anyway as small regions of steep gradient. The solution within this region is of no great physical importance. It serves for bookkeeping purposes to connect the left and right states. For conservative schemes it allows the total mass, momentum and energy in the system to be calculated, and therefore a rough estimate of the shock location can be found by found by inserting the shock at that position which best agrees with these estimates.

Our analysis will focus on the apparently trivial case of a stationary shock in one dimension. It is well-known that for both the exact and Roe's Riemann solver, a stationary shock with one intermediate state exists. That is to say, there exist steady solutions of the discrete equations of the form $\mathbf{u}_L, \ldots \mathbf{u}_L, \mathbf{u}_M, \mathbf{u}_R, \ldots \mathbf{u}_R$ for a one-parameter family of states $\mathbf{u}_M$. The condition that determines these states is that the fluxes computed at the interfaces between $\mathbf{u}_L$ and $\mathbf{u}_M$, and between $\mathbf{u}_M$ and $\mathbf{u}_R$ must equal $\mathbf{f}(\mathbf{u}_L)$ (and also, of course $\mathbf{f}(\mathbf{u}_R)$). For both the Godunov and Roe fluxes, the locus of intermediate states $\mathbf{u}_M$ is the nonphysical branch of the Hugoniot curve through $\mathbf{u}_R$ and are in the interval between $\mathbf{u}_L$ and $\mathbf{u}_R$. We refer to the set of states $\mathbf{u}_M$ as equilibrium states.

Although this family of solutions seems attractive, it has the disadvantage of not defining a unique shock location. Depending on whether we apply conservation of density or energy, we will obtain two different estimates

$$x_S(\rho) = \frac{\rho_M - \rho_R}{\rho_L - \rho_R} \qquad x_S(E) = \frac{E_M - E_R}{E_L - E_R}. \tag{10}$$

These will not be the same, because the Hugoniot locus follows a curve. This is already known, although there does not seem to be any formal publication on the matter. The discrepancy can be exhibited by computing the locus. The jump conditions are applied to a given state $\mathbf{u}_L$ to find the state $\mathbf{u}_R$ behind a stationary shock, and then applied from $\mathbf{u}_R$ to a family of states $\mathbf{u}_M$. The outcome is shown in Figure 2.

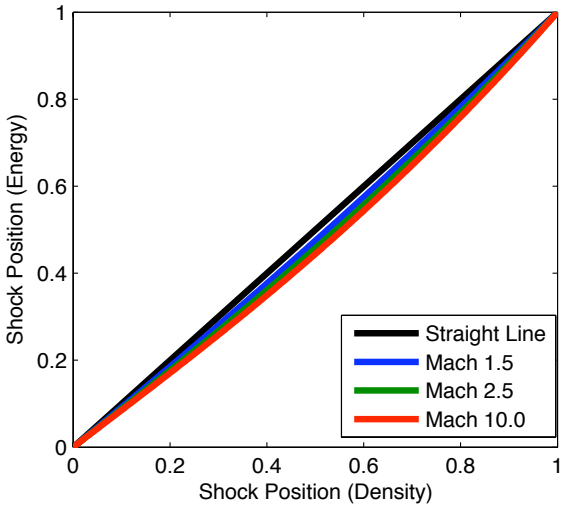

Figure 2: Shock position in energy vs shock position in density in the intermediate cell for initial Mach numbers of 1.5, 2.5, 4.0 and 10.0. The deviation from the straight line represents the ambiguity in shock position.

It turns out that the discrepancy is greater, as might be expected, for stronger shocks, but never exceeds about 5% of the cell size. Nevertheless, it must have consequences. In a blunt body calculation, the shock provides a boundary condition for the subsequent subsonic flow, and this boundary condition will be in error by $\mathcal{O}(\Delta x)$.

The situation is even worse if shock position is computed using momentum, because as the mass flux, it is equal for the left and right states, but not necessarily for the intermediate state. For the exact Riemann solver or Roe's Riemann solver, a momentum spike of as much as 40% is possible, and in general a spike is observed for all flux functions, independent of the number of intermediate states.

Note that if the Hugoniot were linear, there would be no ambiguity. This ambiguity and nonlinearity has previously been related to each anomaly examined [44]. It had been previously noted [4] that the slowly moving shockwave phenomenon was not present for systems with linear Hugoniot curves (Temple systems [46]). Our goal therefore is to make the Euler equations look like a Temple system. We would like to devise a scheme admitting a family of steady shocks with a single intermediate state given by

$$\mathbf{u}_M = \alpha \mathbf{u}_L + (1-\alpha)\mathbf{u}_R. \tag{11}$$

Such a solution would, incidentally, be the projection of the exact solution into the finite-volume space of piecewise constant function.

5 New Flux Functions

We are strongly inclined to believe that the above objective cannot be met by any two-point flux function $\mathbf{f}_{i+\frac{1}{2}} = \mathbf{f}(\mathbf{u}_i, \mathbf{u}_{i+1})$ so that a more general idea of a flux function, $\mathbf{f}_{i+\frac{1}{2}} = \mathbf{f}(\mathbf{u}_{i-m}, \ldots, \mathbf{u}_{i+n})$, rather than a Riemann solver is needed.

We begin by asking what aspects of a typical shock-capturing solution can be trusted, particularly with respect to the intermediate cells. It seems that the conserved quantities should be trusted,

if for no other reason than to preserve conservation of the system. However, we should perhaps not trust the flux values, since these assume that a pressure can be calculated from an equation of state, and this in turn implies assuming thermodynamic equilibrium. That assumption may not be tenable since it does not hold within a real physical shock.

5.1 Interpolated Fluxes

Our idea is to find the fluxes in the untrustworthy intermediate cells by extrapolation from trustworthy neighbors. These interpolated fluxes will be denoted by $\mathbf{f}^*$. The interpolated fluxes are constructed to have the following properties:

1. If the problem is linear so that the Jacobian matrix $\mathbf{A}(\mathbf{u})$ is constant, then $\mathbf{f}_i^* = \mathbf{f}_i$, the interpolated flux equals the equilibrium flux, $\mathbf{f}(\mathbf{u}_i)$. This is a desirable property because the anomalies do not arise for linear systems.

2. If the problem is nonlinear, but the data is smooth, then $\mathbf{f}_i^* = \mathbf{f}_i + \mathcal{O}((\Delta x)^2)$ This property preserves second-order accuracy in smooth regions.

3. If the problem is nonlinear and involves a one-point stationary shock, then $\mathbf{f}_i^*$ is constant, not only on each side of the shock, but also in the intermediate cell, unlike the equilibrium flux. This reflects constancy of the flux in the exact solution, unlike the strong perturbations, especially in momentum, observed in captured shocks.

To begin, suppose the flux is extrapolated from one side as

$$\mathbf{f}_i^* = \mathbf{f}_{i-1} + \tilde{\mathbf{A}}_i(\mathbf{u}_i - \mathbf{u}_{i-1}) \tag{12}$$

for some choice of flux Jacobian, $\tilde{\mathbf{A}}_i$, and extrapolated from the other side as

$$\mathbf{f}_i^* = \mathbf{f}_{i+1} - \tilde{\mathbf{A}}_i(\mathbf{u}_{i+1} - \mathbf{u}_i). \tag{13}$$

These two equations are consistent if

$$\mathbf{f}_{i+1} - \mathbf{f}_{i-1} = \tilde{\mathbf{A}}_i(\mathbf{u}_{i+1} - \mathbf{u}_{i-1}). \tag{14}$$

The simplest matrix having this property is the cell-centered Roe matrix, defined as in section 2.1, but spanning three states rather than two. Averaging Equations (12) and (13) leads to a centered construction of the interpolated flux

$$\mathbf{f}_i^* = \frac{1}{2}(\mathbf{f}_{i-1} + \mathbf{f}_{i+1}) - \frac{1}{2}\tilde{\mathbf{A}}_{i-1,i+1}(\mathbf{u}_{i+1} - 2\mathbf{u}_i + \mathbf{u}_{i-1}). \tag{15}$$

With the definition in place, it is simple to show that for a captured stationary shock having one intermediate state with no positional ambiguity (11) , the interpolated flux is identical everywhere. While it is clear that a non-monotone shock structure ($\alpha < 0$ or $\alpha > 1$) will also lead to the same result, this results in a rarefaction shock at either the left-middle or middle-right edge. Any measure that eliminates rarefaction shocks will therefore eliminate the non-monotone solutions.

The effect of the interpolation can be seen by taking a Taylor series expansion of the centered form in Equation (15);

$$\mathbf{f}_i^* = \mathbf{f}_i + \frac{(\Delta x)^2}{2}\mathbf{A}_x\mathbf{u}_x + \mathcal{O}((\Delta x)^4) = \mathbf{f}_i + \frac{1}{2}(\Delta\mathbf{A})(\Delta\mathbf{u}) + \mathcal{O}((\Delta x)^4), \tag{16}$$

which is a modification to the flux proportional to the product of the derivatives of the flux Jacobian and conserved variables. The modification vanishes if $\mathbf{A}$ is constant, is second-order in smooth regions, but is order unity near nonlinear shocks. It also vanishes across stationary contacts. The next task is to devise a numerical scheme that exploits these properties.

5.2 New Flux Function - A

With interpolated fluxes introduced, we define a new flux function that can be described similar to the original Roe framework, referred to as new flux function A,

$$\mathbf{f}^A_{i+\frac{1}{2}} = \frac{1}{2}(\mathbf{f}^*_i + \mathbf{f}^*_{i+1}) - \frac{1}{2}\text{sign}(\tilde{\mathbf{A}}_{i+\frac{1}{2}})(\mathbf{f}^*_{i+1} - \mathbf{f}^*_i) \tag{17}$$

with Roe's Riemann solver obtained if $\mathbf{f}^*_i = \mathbf{f}_i$. This ensures that the new method recovers Roe's method for linear problems.

Flux function A can be expanded as

$$\begin{aligned}\mathbf{f}^A_{i+\frac{1}{2}} &= \frac{1}{2}(\mathbf{f}_{i+1} + \mathbf{f}_i) - \frac{1}{2}|\tilde{\mathbf{A}}_{i+\frac{1}{2}}|(\mathbf{u}_{i+1} - \mathbf{u}_i) + \frac{1}{2}\Big((\mathbf{I} - \text{sign}(\tilde{\mathbf{A}}_{i+\frac{1}{2}}))\tilde{\mathbf{A}}_{i+1} \\ &\quad -(\mathbf{I} + \text{sign}(\tilde{\mathbf{A}}_{i+\frac{1}{2}}))\tilde{\mathbf{A}}_i + 2|\tilde{\mathbf{A}}_{i+\frac{1}{2}}|\Big)(\mathbf{u}_{i+1} - \mathbf{u}_i).\end{aligned} \tag{18}$$

The first two terms in Equation (18) are Roe's original solver and the third term contains a "viscosity"-like matrix proportional to $\partial_x \mathbf{A} \partial_x \mathbf{u}$.

There is one obvious issue with this formulation, through the diffusion component of the Riemann solver, $\text{sign}(\tilde{\mathbf{A}}_{i+\frac{1}{2}})(\mathbf{f}^*_{i+1} - \mathbf{f}^*_i)$. In this term, since the interpolated flux difference is computed with different quantities than the flux Jacobian and the sign function is discontinuous, the flux function is not continuous either.

5.3 New Flux Function - B

To overcome the difficulty of new flux function A, another flux function, B, can be written as

$$\mathbf{f}^B_{i+\frac{1}{2}} = \frac{1}{2}(\mathbf{f}^*_i + \mathbf{f}^*_{i+1}) - \frac{1}{2}|\overline{\mathbf{A}}_{i+\frac{1}{2}}|(\mathbf{u}_{i+1} - \mathbf{u}_i) \tag{19}$$

where $\overline{\mathbf{A}}_{i+\frac{1}{2}}$ is the Roe matrix across cells $i-1$ and $i+2$,

$$\overline{\mathbf{A}}_{i+\frac{1}{2}}(\mathbf{u}_{i+2} - \mathbf{u}_{i-1}) = \mathbf{f}_{i+2} - \mathbf{f}_{i-1} \tag{20}$$

An intuitive interpretation is that the matrix $\overline{\mathbf{A}}$ "explains" the difference of states $\mathbf{u}_{i+1} - \mathbf{u}i$ from the viewpoint of a "bigger picture". It is easy to show that this flux function allows for a one-point stationary shock if the intermediate state is collinear with the end states in state space. In such a situation, at every interface, the difference in conserved variables is either zero or a null vector of the Roe matrix that spans the left and right states. Just like flux function A, this reduces to Roe's Riemann solver for a single jump in data. For this function, an entropy fix is more traditional since it can be included directly within the Roe matrix. Flux function B can also be written as a

correction to Roe's Riemann solver as

$$\begin{aligned}\mathbf{f}^B_{i+\frac{1}{2}} &= \frac{1}{2}(\mathbf{f}_i + \mathbf{f}_{i+1}) - \frac{1}{2}|\tilde{\mathbf{A}}_{i+\frac{1}{2}}|(\mathbf{u}_{i+1} - \mathbf{u}_i) \\ &\quad + \frac{1}{2}\left(|\tilde{\mathbf{A}}_{i+\frac{1}{2}}| + \tilde{\mathbf{A}}_{i+1} - \tilde{\mathbf{A}}_i - |\overline{\mathbf{A}}_{i+\frac{1}{2}}|\right)(\mathbf{u}_{i+1} - \mathbf{u}_i). \end{aligned} \tag{21}$$

Physically speaking, both new functions trust the values of the conserved quantities, but do not necessarily trust the equilibrium flux functions, and evaluate them differently in the vicinity of a shock.

6 Burgers' Equation

It is instructive to apply the new method to Burgers' equation because, even though there are no anomalies to be cured in that case (or any scalar case), some very simple analysis can be carried out to see if any adverse effects arise. The equation is

$$u_t + f_x = u_t + \left(\frac{1}{2}u^2\right)_x. \tag{22}$$

Shockwaves are represented by the jump conditions $\Delta(\frac{1}{2}u^2) = S\Delta u$ and move with speed $S = \frac{1}{2}(u_L + u_R)$. The Roe-averaged velocity is just the arithmetic average, $\tilde{u} = \frac{1}{2}(u_L + u_R)$. Since there is only variable, there can be no ambiguity in shock position and thus no anomalous behavior. The interpolated flux for this system is

$$f^*_i = \frac{1}{2}[u_i(u_{i+1} + u_{i-1}) - u_{i-1}u_{i+1}]. \tag{23}$$

It is possible for this flux to be be negative and therefore not realizable. This will happen if

$$\frac{(u_{i+1} + u_{i-1})u_i}{u_{i+1}u_{i-1}} < 1, \tag{24}$$

represented by the unshaded part of Figure 3 as a function of the ratios of data from neighboring cells, u_{i-1}/u_i and u_{i+1}/u_i. Clearly such data will only arise exceptionally, but future work will need to investigate any analogous behavior in the Euler equations.

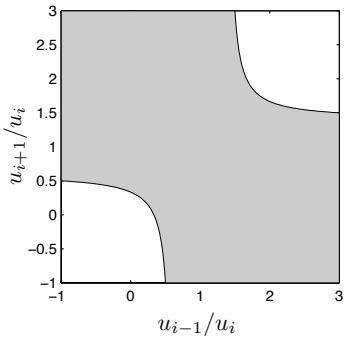

Figure 3: Physically realizable region of interpolated flux for Burgers' Equation

6.1 Total Variation Diminishing

First introduced by Harten [47] total variation diminishing (TVD) is a property of numerical schemes that ensures they preserve monotonicity and do not create local extrema. Defining the discrete total variation as

$$TV(u) = \sum_i |u_i - u_{i-1}|, \tag{25}$$

a method is TVD if

$$TV(u^{n+1}) \leq TV(u^n). \tag{26}$$

The approach we use to determine whether the new flux functions are TVD is based on the original work of Harten [48]. The flux functions are said to be TVD if

$$\frac{\Delta t}{\Delta x}\left|\frac{f^*_{i+1} - f^*_i}{u_{i+1} - u_i}\right| \leq q^*_{i+\frac{1}{2}} \leq 1 \tag{27}$$

is satisfied, where $q^*_{i+\frac{1}{2}}$ is the numerical viscosity coefficient obtained by writing the flux function in the form

$$f_{i+\frac{1}{2}} = \frac{1}{2}(f^*_i + f^*_{i+1}) - \frac{1}{2}\frac{\Delta x}{\Delta t} q^*_{i+\frac{1}{2}}(u_{i+1} - u_i). \tag{28}$$

This condition for TVD simplifies to

$$\frac{1}{2}\frac{\Delta t}{\Delta x}\left|u_{i+2} + u_{i-1}\right| \leq q^*_{i+\frac{1}{2}} \leq 1 \tag{29}$$

and the new flux functions can be checked. For flux function A, the viscosity coefficient is

$$q^{*,A}_{i+\frac{1}{2}} = \frac{1}{2}\frac{\Delta t}{\Delta x}\text{sign}(u_{i+1} + u_i)(u_{i+2} + u_{i-1}) \tag{30}$$

and the lower bound of Equation (29) reduces to

$$|(u_{i+2} + u_{i-1})| \leq \text{sign}(u_{i+1} + u_i)\text{sign}(u_{i+2} + u_{i-1})\left|(u_{i+2} + u_{i-1})\right|. \tag{31}$$

and thus flux function A is not TVD, since this condition does not hold for all data. For flux function B, the viscosity coefficient is

$$q^{*,B}_{i+\frac{1}{2}} = \frac{1}{2}\frac{\Delta t}{\Delta x}|u_{i-1} + u_{i+2}| \tag{32}$$

and the lower bound of Equation (29) is trivially satisfied, therefore flux function B is TVD by this approach. For both flux functions, the upper bound is a CFL-like condition and can be satisfied through the proper choice of timestep.

This analysis demonstrates an advantage of flux function B and suggests where changes to flux function A need to be made to prevent the growth of solution extrema. The results from analysis of the interpolated flux from both a physicality and TVD perspective strongly point towards interpolated fluxes only being used if the data is monotone. At this point, since this is just a scalar result (and a scalar property), it is not clear which variables should be monotone in a system of equations, but is definitely worth considering in the future development and understanding of both new flux functions.

7 Numerical Results

7.1 Stationary Shocks

Both methods A and B are designed to capture stationary shocks with one intermediate point described by (11) and indeed they did. It does need to be asked, however, whether those solutions are stable. It was established by Barth, and by Serre [21, 22], that the one-point shocks produced by the Godunov and Roe methods are not always stable. The instability happens for strong enough shocks, over a range of shock locations. Depending on the boundary conditions, the shock will either move to a stable position or enter an approximate limit cycle. This behavior has been called a "one-dimensional carbuncle". No evidence of this was found in experiments, and this was confirmed by a numerical eigenvalue analysis, along the lines conducted by Barth.

Starting with a one-point stationary shock, the residual function corresponding to the net flux through the intermediate state is

$$\mathbf{r}(\mathbf{u}_M; \mathbf{u}_L, \mathbf{u}_R) = \mathbf{f}_{MR} - \mathbf{f}_{LM} \tag{33}$$

for the shock with left and right endpoints $\mathbf{u}_L$ and $\mathbf{u}_R$. This function has a zero eigenvalue and a singular Jacobian matrix, $\det\left[\frac{\partial \mathbf{r}}{\partial \mathbf{u}_M}\right] = 0$, since all middle states $\mathbf{u}_M$ are stationary points. To determine the sensitivity to the zero eigenvalue, examine the semi-discrete equations on a grid with unit spacing,

$$\frac{\partial \mathbf{u}_M}{\partial t} + \mathbf{r}(\mathbf{u}_M; \mathbf{u}_L, \mathbf{u}_R) = \mathbf{0}. \tag{34}$$

Near a stationary solution, $\mathbf{u}^*$, the residual, $\mathbf{r}(\mathbf{u}^*; \mathbf{u}_L, \mathbf{u}_R)$, is zero and the residual can be linearized with $\mathbf{u}_M = \delta\mathbf{u} + \mathbf{u}^*$ as

$$\mathbf{r}(\mathbf{u}_M) = \mathbf{r}(\mathbf{u}^* + \delta\mathbf{u}) = \mathbf{r}(\mathbf{u}^*) + \frac{\partial \mathbf{r}(\mathbf{u}^*)}{\partial \mathbf{u}_M}\delta\mathbf{u} \tag{35}$$

such that $\delta\mathbf{u}$ is governed by

$$\frac{\partial(\delta\mathbf{u})}{\partial t} + \frac{\partial \mathbf{r}(\mathbf{u}^*)}{\partial \mathbf{u}_M}\delta\mathbf{u} = 0 \tag{36}$$

and the solution can be determined from the eigenvalues, λ_i, and eigenvectors, $\mathbf{r}_i$, of the residual Jacobian,

$$\delta\mathbf{u}(t) = \alpha_1\mathbf{r}_1 + \alpha_2\mathbf{r}_2 e^{-\lambda_2 t} + \alpha_3\mathbf{r}_3 e^{-\lambda_3 t} \tag{37}$$

where λ_1 corresponds to the stationary eigenvalue and is zero. Stability and carbuncle free requires $\lambda_2, \lambda_3 \geq 0$ to ensure the stability of $\mathbf{u}_M$. To avoid boundary effects, the eigenvalues of $\frac{\partial \mathbf{r}}{\partial \mathbf{u}}$ are examined for a stationary shock problem using several extra cells. For this analysis, the initial middle state is created on the nonphysical branch of the Hugoniot for Roe's Riemann solver and on a straight line in state space for the new flux functions. The results are shown in Figure 4 for Roe's flux function and both new flux functions. At Mach 10 and 20, negative eigenvalues are seen only for the Roe flux. From this analysis, both new flux functions are carbuncle-free in one dimension.

7.2 The Slowly Moving Shock Phenomenon

Our analysis has been based on the case of a stationary shock, for which the locus of steady intermediate states is either the nonphysical Hugoniot (Godunov, Roe) ar a straight line (Methods A and B). We have confirmed the following by numerical experiment; If a captured shock moves sufficiently slowly with speed $S \ll 1$, across the grid, the profile at any particular instant is very close to one of the stationary solutions. Hence, with our modified methods, the state in any particular

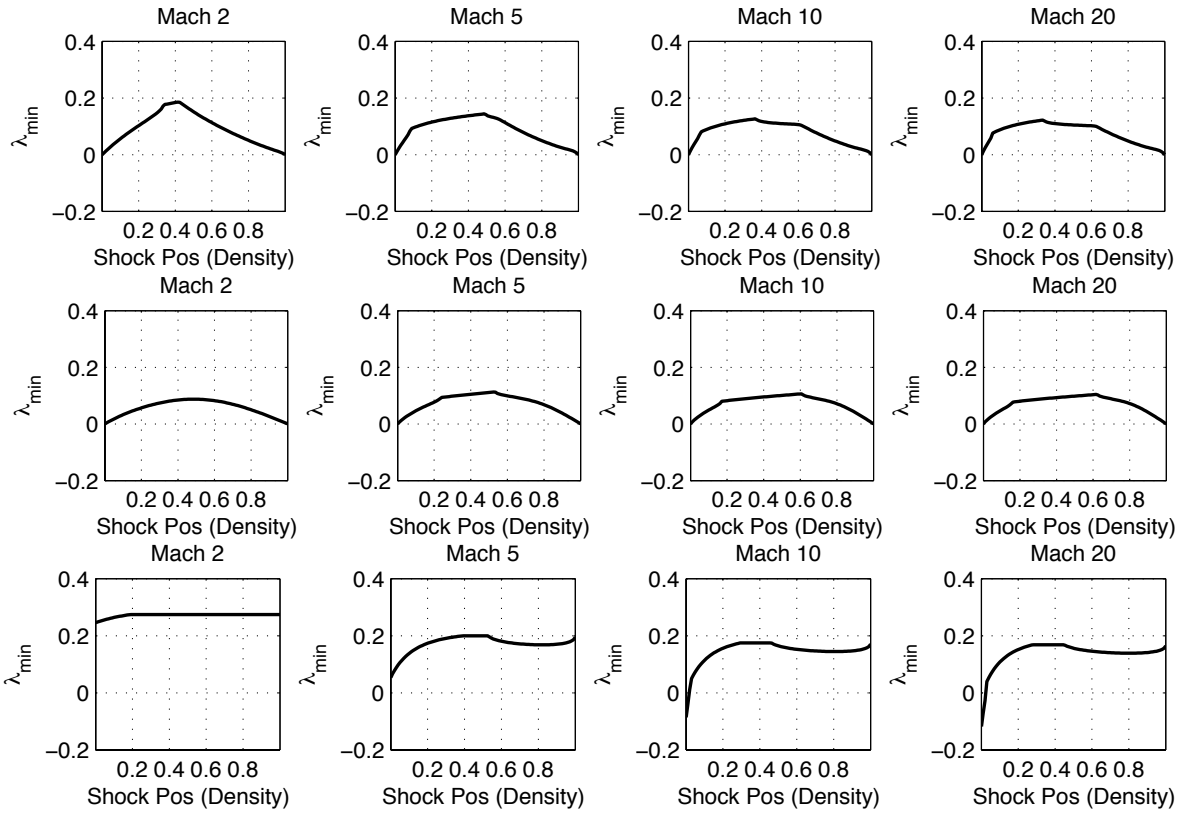

Figure 4: Stability Results for the one-dimensional carbuncle for flux function A (top), flux function B (middle), Roe's Flux (bottom) for 4 different Mach numbers. Only Roe's Flux has negative (unstable) eigenvalues.

cell remains constant at $\mathbf{u}_R$ and then ramps up linearly to $\mathbf{u}_L$ in time $\Delta x/S$.

As the shock speed is increased, there are departures from this ideal behavior. We conduct numerical experiments on a Mach 10 shock, varying the frame of reference to contain different shock speeds.

Looking at the results in Figure 5 for the slowest shock speed, both new fluxes greatly reduce the momentum spike in the slowly moving shock. Flux function A appears to completely remove it, while flux function B leaves a very small spike behind. Of utmost importance is that the new flux functions have not smeared out the shockwave - there is still only one intermediate state at any particular time. The state space plots demonstrate the linearly placed intermediate shock states. It is clear that the ambiguity in shock position has been dramatically reduced. This is expected, since in this case, the shock is very close to stationary.

For a slightly faster shock, in Figure 6, both fluxes again significantly reduce the momentum spike and perform well, although the difference between flux function A and flux function B is clearer. For this problem, flux function A maintains a much more linear shock profile than flux function B. For an even faster shock in Figure 7, the momentum spike with Roe's flux is smaller and the anomalous behavior is less pronounced. Combining all these results and looking specifically at the momentum, where the largest error is observed, leads to Figure 8. In this figure, the error is defined as

$$\text{Relative Maximum Momentum Error } = \frac{\max_{x,t}(\rho u) - \rho_R u_R}{\rho_R u_R} \times 100, \tag{38}$$

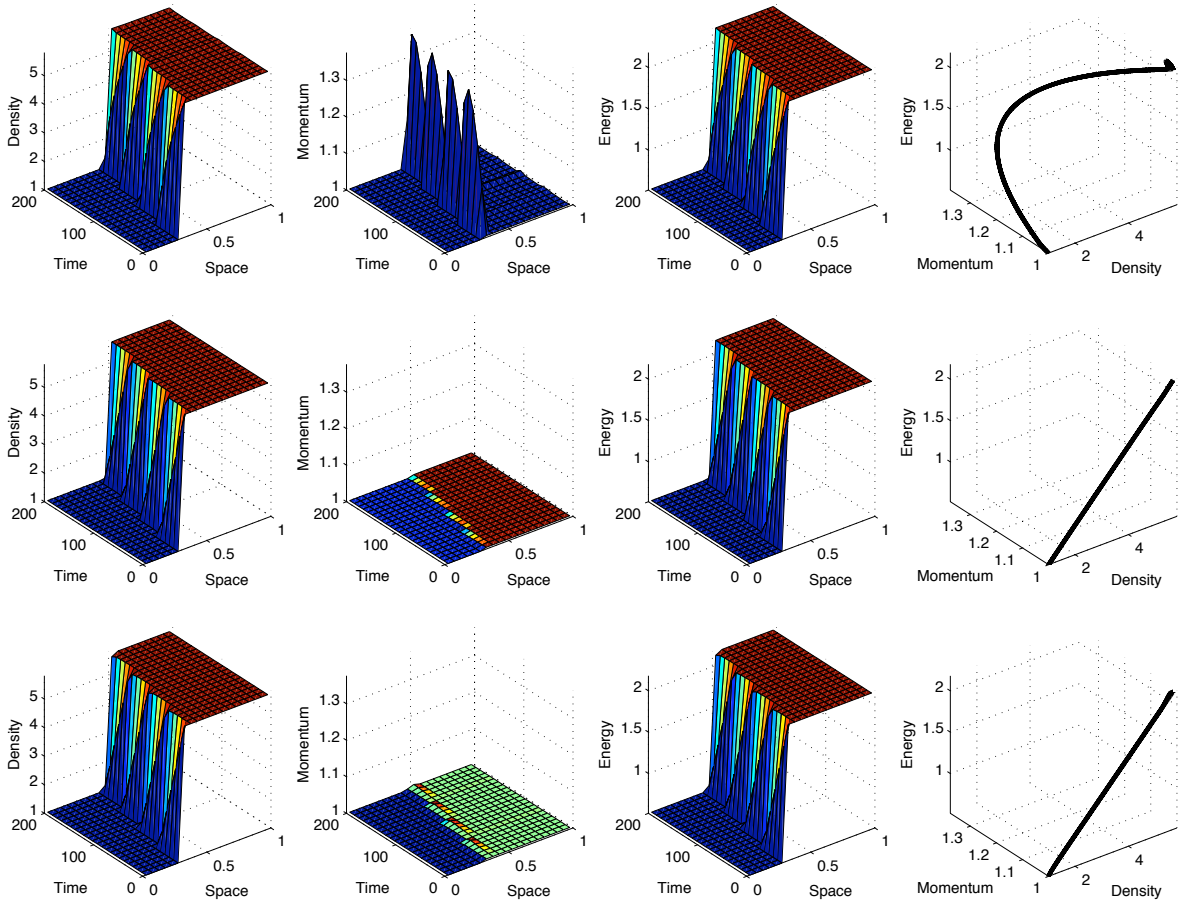

Figure 5: Results for the slowly moving shock problem with $S = 0.0001$. (top) Roe's Riemann Solver. (middle) Flux function A. (bottom) Flux function B. For each flux, density, momentum, and energy are shown as a function of space and time. On the right, the results are plotted in conserved state space.

which is a measure of the momentum overshoot. Flux function A reduces the error the most, outperforming flux function B on this problem for all Mach numbers.

7.2.1 Wall Heating

With the strong performance on the slowly moving shock phenomenon, the new fluxes are tested on the Noh Problem. The initial data is $\mathbf{u}_0 = (\rho_0, -\rho_0 u_0, E_0)^T$ but can be reduced to a one parameter family with Mach number as the free parameter and

$$\rho_0 = 1, \qquad u_0 = 1, \qquad p_0 = \frac{1}{\gamma M_0^2}. \tag{39}$$

The solution behind the shock can be determined exactly from the jump conditions as

$$\rho = 1 + \frac{1}{S}, \qquad u = 0, \qquad p = p_0 + (1 + S), \tag{40}$$

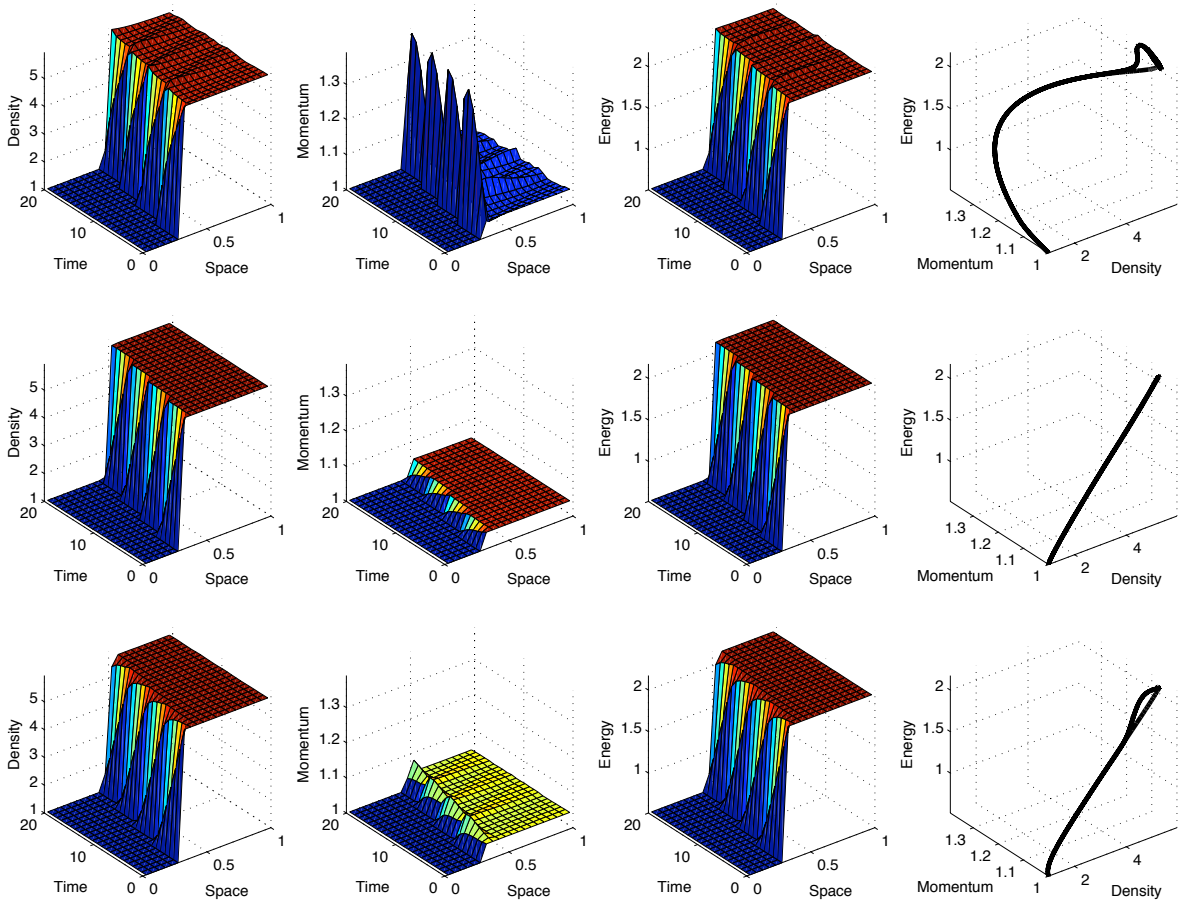

Figure 6: Results for the slowly moving shock problem with $S = 0.001$. Same plots as Figure 5.

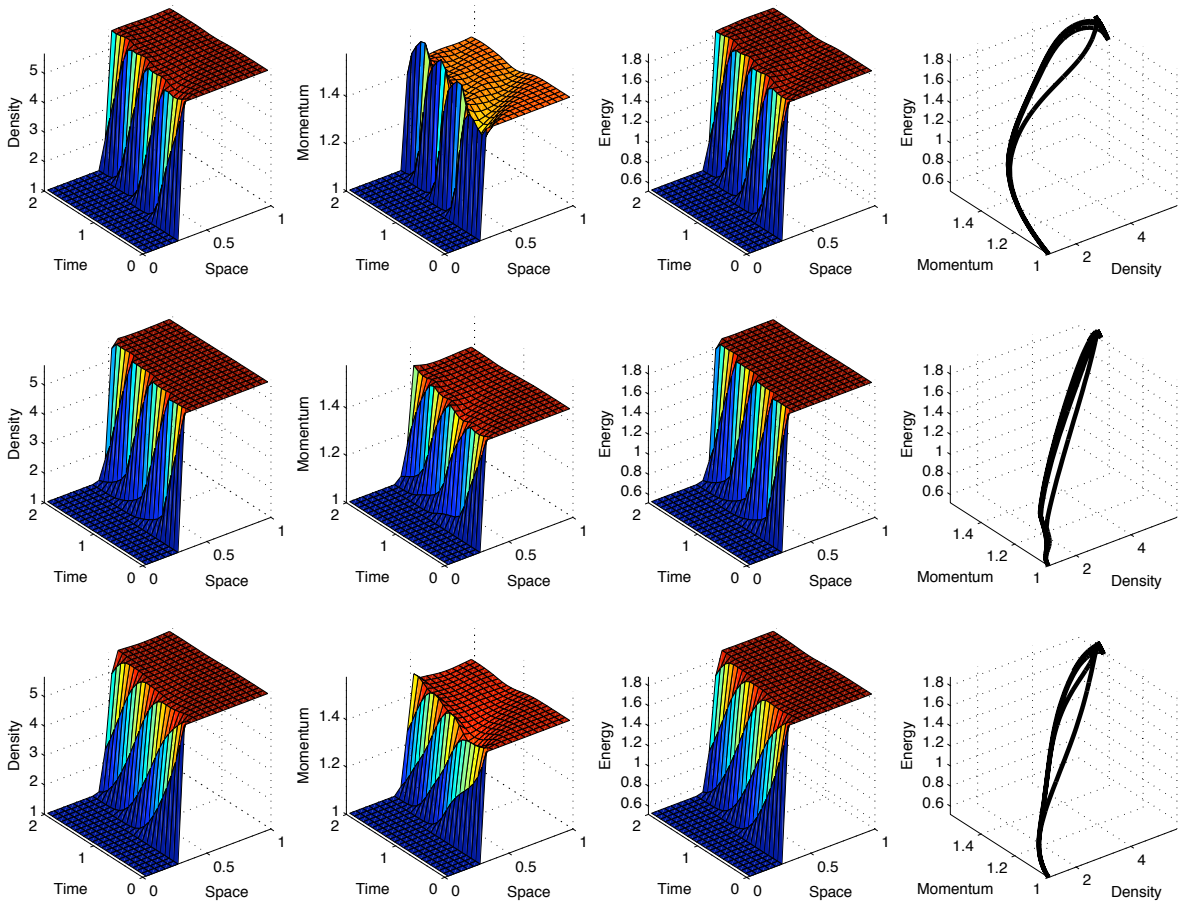

Figure 7: Results for the slowly moving shock problem with $S = 0.1$. Same plots as Figure 5.

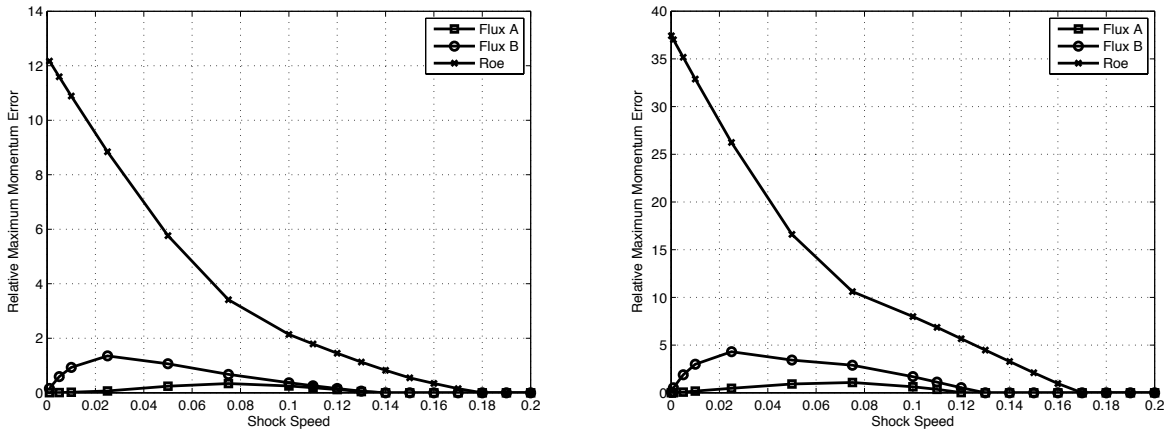

Figure 8: Relative Maximum Momentum Error vs Shock Speed for Roe's Riemann Solver ($\times$), flux function A ($\square$), and flux function B ($\circ$) for Mach 2.0 (left) and Mach 10.0 (right). Both new flux functions reduce the momentum spike significantly for all shock speeds.

with shock speed

$$S = \frac{1}{4}\left((\gamma - 3) + \sqrt{(\gamma+1)^2 + 16\gamma p_0}\right). \tag{41}$$

Results are shown for a CFL number of 0.5. While there is some dependency on CFL number, the trends displayed and overall performance remains the same. Comparing the new fluxes to Roe's Riemann solver in Figure 9, all three methods compute velocity and pressure equivalently. Looking at the density defect at the wall, flux function A dramatically outperforms flux function B, especially for the Mach 10 shock. Looking at the relative wall density error, defined as

$$\text{Relative Wall Density Error } = \frac{\rho_{wall} - \rho_{exact}}{\rho_{exact}} \times 100 \tag{42}$$

in Figure 10 shows that for all Mach numbers, flux function A reduces the error significantly while flux function B performs comparably to Roe's Riemann solver, reducing the density defect slightly in comparison. Thus reducing the ambiguity in shock position can reduce the density defect at the wall. The improvement is greatest at higher Mach numbers, when the shock speed is slowest.

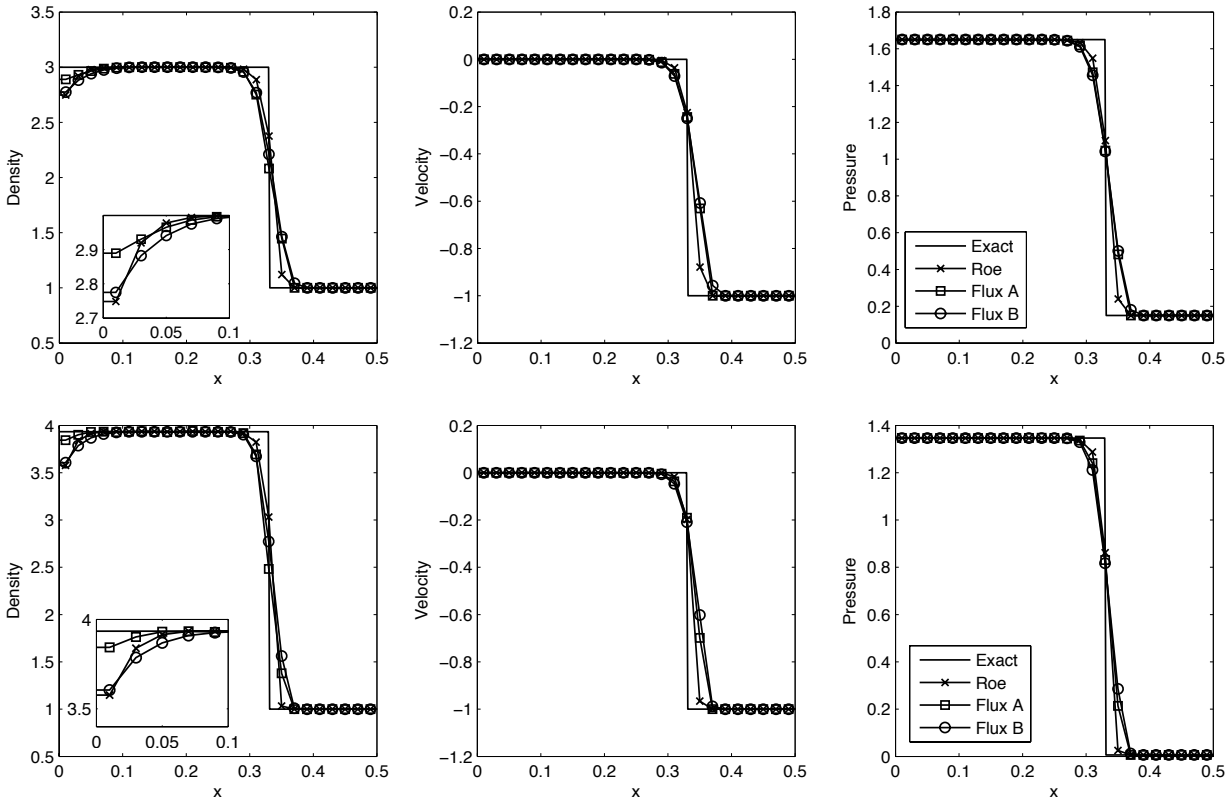

Figure 9: Density, velocity and pressure results for the Noh problem with initial Mach number of 2 (top) and Mach number of 10 (bottom).

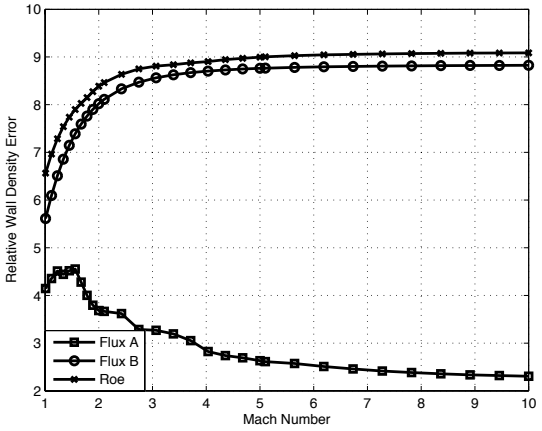

Figure 10: Relative Wall Density Error vs Mach number for Roe's Riemann Solver ($\times$), flux function A ($\square$), and flux function B ($\circ$).

8 Conclusions and Future Work

All captured shocks contain intermediate states between their end states. These intermediate states should not be taken literally; in particular it should not be assumed that they are in local thermodynamic equilibrium. Using the equilibrium equation of state for these intermediate states gives rise to intermediate states which differ from the projection of the exact solution into cell averages and to an ambiguity in the shock location. This ambiguity is linked to much of the anomalous behavior in shock-capturing schemes, represented by three canonical examples: the wall heating phenomenon, the slowly moving shock phenomenon, and the carbuncle. To eliminate the ambiguity, the intermediate states must agree on the location of the shock.

We introduced the idea of interpolated fluxes and two new flux functions were developed to utilize them and provide an unambiguous stationary shock structure. The first one, flux function A, is constructed based on the flux-wave approach [49] - decomposing the Riemann problem into jumps in interpolated flux across each wave, using wavespeeds to determine the direction of their contribution to the interface flux. The second one, flux function B, is based on the classical Roe Riemann solver, again using interpolated fluxes but relying on conserved variables to determine the jumps across each wave and the contribution of each wave to the interface flux.

On all of the shock anomalies in one-dimension, both fluxes showed improvement on existing methods without noticeably smearing or diffusing the shock. For a range of other canonical problems, there was no major detriment to using the flux functions outside of shockwaves since they reduce to a second-order correction to Roe's Riemann solver and the differences were not observed in the first-order framework.

There are numerous other possible flux formulae, based on the interpolated fluxes, able to preserve the same desirable steady shock structures, and these will be investigated. However, the most urgent task is to extend the work to higher dimensions. A starting point for this is to consider a stationary shockwave oblique to the mesh. We can declare that no cell intersected by this shock is trustworthy, and try to replace the flux in such cells by interpolations, all of which should lie on the straight line in state space that joins the preshock and postshock states. A simple method for doing this has yet to be devised.

References

[1] I G Cameron. An analysis of the errors caused by using artificial viscosity terms to represent steady-state shock waves. *Journal of Computational Physics*, 1:1–20, 1966.

[2] A Emery. An evaluation of several differencing methods for inviscid fluid flow problems. *Journal of Computational Physics*, 2:306–331, 1968.

[3] Thomas W Roberts. The behavior of flux difference splitting schemes near slowly moving shock waves. *Journal of Computational Physics*, 90(1):141–160, 1990.

[4] Mohit Arora and Philip L Roe. On postshock oscillations due to shock capturing schemes in unsteady flows. *Journal of Computational Physics*, 130(1):25–40, 1997.

[5] Shi Jin and Jian-Guo Liu. Oscillations induced by numerical viscosities. *Mat. Contemp*, 10:169–180, 1995.

[6] Shi Jin and Jian-Guo Liu. The effects of numerical viscosities: I. slowly moving shocks. *Journal of Computational Physics*, 126(2):373–389, 1996.

[7] G Efraimsson and G Kreiss. A note on the effect of artificial viscosity on solutions of conservation laws. *Applied Numerical Mathematics*, 21:155–173, 1996.

[8] Smadar Karni and Suncica Canic. Computations of slowly moving shocks. *Journal of Computational Physics*, 136(1):132–139, 1997.

[9] K Xu and J Hu. Projection dynamics in godunov-type schemes. *Journal of Computational Physics*, 142(2):412–427, 1998.

[10] Y Stiriba and R Donat. A numerical study of postshock oscillations in slowly moving shock waves. *Computers & Mathematics with Applications*, 46(5-6):719–739, 2003.

[11] Eric Johnsen and S K Lele. Numerical errors generated in simulations of slowly moving shocks. *Center for Turbulence Research, Annual Research Briefs*, pages 1–12, 2008.

[12] Eric Johnsen, Sanjiva K Lele, and Johan Larsson. Analysis and correction of errors generated by slowly moving shocks. *Proceedings of the 49th AIAA Aerospace Sciences Meeting*, 2011.

[13] Kun Xu. Does perfect riemann solver exist? *Proceedings of the 14th AIAA Computational Fluid Dynamics Conference*, 1999.

[14] KM Peery and ST Imlay. Blunt-body flow simulations. *AIAA paper*, pages 88–2924, 1988.

[15] K Kitamura, E Shima, and PL Roe. Three-dimensional carbuncles and euler fluxes. *Proceddings of the 48th AIAA Aerospace Sciences Meeting*, 2010.

[16] JJ Quirk and S Karni. On the dynamics of a shock–bubble interaction. *Journal of Fluid Mechanics*, 318:129–163, 1996.

[17] Y Chauvat, JM Moschetta, and J Gressier. Shock wave numerical structure and the carbuncle phenomenon. *International Journal for Numerical Methods in Fluids*, 47(8âĂŘ9):903–909, 2005.

[18] Keiichi Kitamura, Philip L Roe, and Farzad Ismail. Evaluation of euler fluxes for hypersonic flow computations. *AIAA Journal*, 47(1):44–53, 2008.

[19] SP D'yakov. Shock wave stability. *Zh. Eksp. Teor. Fiz*, page 288, 1954.

[20] LD Landau and EM Lifshitz. Fluid mechanics. *Pergammon*, 1959.

[21] Timothy J Barth. Some notes on shock resolving flux functions. part 1: Stationary characteristics. *NASA Technical Memorandum*, 1989.

[22] Matthieu Bultelle, Magali Grassin, and Denis Serre. Unstable godunov discrete profiles for steady shock waves. *SIAM Journal on Numerical Analysis*, 35(6):2272–2297, 1998.

[23] JC Robinet, J Gressier, G Casalis, and JM Moschetta. Shock wave instability and the carbuncle phenomenon: same intrinsic origin? *Journal of Fluid Mechanics*, 417:237–263, 2000.

[24] M Pandolfi and D D'Ambrosio. Numerical instabilities in upwind methods: analysis and cures for the "carbuncle" phenomenon. *Journal of Computational Physics*, 166(2):271–301, 2001.

[25] Michael Dumbser, Jean-Marc Moschetta, and Jeremie Gressier. A matrix stability analysis of the carbuncle phenomenon. *Journal of Computational Physics*, 197(2):647–670, 2004.
[26] A Bressan, HK Jenssen, and P Baiti. An instability of the godunov scheme. *Communications on Pure and Applied Mathematics*, 59(11):1604–1638, 2006.
[27] Farzad Ismail. Toward a reliable prediction of shocks in hypersonic flow: resolving carbuncles with entropy and vorticity control. *Ph.D. Thesis*, 2006.
[28] M V C Ramalho, J H A Azevedo, and J L F Azevedo. Further investigation into the origin of the carbuncle phenomenon in aerodynamic simulations. *Proceedings of the 49th AIAA Aerospace Sciences Meeting*, 2011.
[29] Meng-Sing Liou. Mass flux schemes and connection to shock instability. *Journal of Computational Physics*, 160:623–648, 2000.
[30] R Menikoff. Numerical anomalies mimicking physical effects. *AIP Conference Proceedings*, 1996.
[31] P Roe, H Nishikawa, F Ismail, and L Scalabrin. On carbuncles and other excrescences. *Proceedings of the 17th AIAA Computational Flow Dynamics Conference*, pages 1–10, 2005.
[32] Volker Elling. The carbuncle phenomenon is incurable. *Acta Mathematica Scientia, Series B*, 29(6):1647–1656, 2010.
[33] B I Rodzhestvenskii and N N Yanenko. Systems of quasilinear equations and their applications to gas dynamics. *AMS Translation*, 1983.
[34] Philip L Roe and Daniel W Zaide. Entropy traces in lagrangian and eulerian calculations. *Proceedings of the 7th International Conference on Computational Fluid Dynamics*, 2010.
[35] William F Noh. Errors for calculations of strong shocks using an artificial viscosity and an artificial heat flux. *Journal of Computational Physics*, 72(1):78–120, 1987.
[36] P Glaister. An approximate linearised riemann solver for the euler equations for real gases. *Journal of Computational Physics*, 74:382–408, 1988.
[37] CD Munz. On godunov-type schemes for lagrangian gas dynamics. *SIAM Journal on Numerical Analysis*, 31(1):17–42, 1994.
[38] Rosa Donat and Antonio Marquina. Capturing shock reflections: an improved flux formula. *Journal of Computational Physics*, 125:42–58, 1996.
[39] RP Fedkiw, A Marquina, and B Merriman. An isobaric fix for the overheating problem in multimaterial compressible flows. *Journal of Computational Physics*, 148(2):545–578, 1999.
[40] M Gehmeyr, B Cheng, and D Mihalas. Noh's constant-velocity shock problem revisited. *Shock Waves*, 7(5):255–274, 1997.
[41] WH Hui and S Kudriakov. On wall overheating and other computational difficulties of shock-capturing methods. *Computational Fluid Dynamics Journal*, 10(2):192–209, 2001.
[42] W Rider. Revisiting wall heating. *Journal of Computational Physics*, 162:395–410, 2000.
[43] Eleuterio F Toro. Anomalies of conservative methods: analysis, numerical evidence and possible cures. *Computational Fluid Dynamics Journal*, 11(2):128–143, 2002.
[44] Daniel W Zaide and Philip L Roe. Shock capturing anomalies and the jump conditions in one dimension. *Proceedings of 20th AIAA Computational Fluid Dynamics Conference, 2011-3686*, 2011.
[45] R Courant and K Friedrichs. Supersonic flow and shock waves. *Interscience*, 1948.
[46] Blake Temple. Systems of conservation laws with invariant submanifolds. *Transactions of the Americal Mathematical Society*, 280(2):781–795, 1983.
[47] A Harten. High resolution schemes for hyperbolic conservation laws. *Journal of Computational Physics*, 49:357–393, 1983.
[48] Edwige Godlewski and Pierre-Arnaud Raviart. Hyperbolic systems of conservation laws. *Mathematiques & Applications*, 1991.

[49] R LeVeque. Wave propagation algorithms for multidimensional hyperbolic systems. *Journal of Computational Physics*, 131(2):327–353, 1997.